AGU PUBLICATIONS

JGR

Journal of Geophysical Research: Atmospheres

RESEARCH ARTICLE
10.1002/2013JD021385

Key Points:
- Concentric gravity waves were observed by CIPS in PMCs
- Concurrent AIRS observations show concentric GWs in the stratosphere
- Convection cannot account for all the observed concentric GWs in PMCs

Correspondence to:
J. Yue,
jia.yue@hamptonu.edu

Citation:
Yue, J., B. Thurairajah, L. Hoffmann, J. Alexander, A. Chandran, M. J. Taylor, J. M. Russell III, C. E. Randall, and S. M. Bailey (2014), Concentric gravity waves in polar mesospheric clouds from the Cloud Imaging and Particle Size experiment, *J. Geophys. Res. Atmos.*, *119*, 5115–5127, doi:10.1002/2013JD021385.

Received 17 DEC 2013
Accepted 10 APR 2014
Accepted article online 13 APR 2014
Published online 6 MAY 2014

Concentric gravity waves in polar mesospheric clouds from the Cloud Imaging and Particle Size experiment

Jia Yue[1], Brentha Thurairajah[2], Lars Hoffmann[3], Joan Alexander[4], Amal Chandran[5], Michael J. Taylor[6], James M. Russell III[1], Cora E. Randall[7], and Scott M. Bailey[2]

[1]Atmospheric and Planetary Science, Hampton University, Hampton, Virginia, USA, [2]Bradley Department of Electrical and Computer Engineering, Virginia Polytechnic Institute and State University, Blacksburg, Virginia, USA, [3]Jülich Supercomputing Centre, Forschungszentrum Jülich, Jülich, Germany, [4]NorthWest Research Associates, Boulder, Colorado, USA, [5]Geophysical Institute, University of Alaska Fairbanks, Fairbanks, Alaska, USA, [6]Center for Atmospheric and Space Sciences, Utah State University, Logan, Utah, USA, [7]Laboratory for Atmospheric and Space Physics and Department of Atmospheric and Oceanic Sciences, University of Colorado, Boulder, Colorado, USA

Abstract Five concentric atmospheric gravity wave (AGW) events have been identified in Polar Mesospheric Cloud (PMC) images of the summer mesopause region (~82–84 km) made by the Cloud Imaging and Particle Size (CIPS) instrument on board the Aeronomy of Ice in the Mesosphere satellite during the Northern Hemisphere 2007 and 2009 PMC seasons. The AGWs modulate the PMC albedo, ice water content, and particle size, creating concentric ring patterns. On only one occasion (13 July 2007), the concentric AGWs in PMCs were aligned with AGWs with similar shapes observed in 4.3 μm radiance in the lower stratosphere, as measured by Atmospheric Infrared Sounder (AIRS). Coincident AIRS and Infrared Atmospheric Sounding Interferometer nadir measurements of 8.1 μm radiance reveal a region of deep convection in the troposphere close to the estimated centers of the AGWs in the stratosphere, strongly suggesting that convection is the wave source. The AGWs in CIPS on 13 July 2007 were ~1000 km away from the observed deep convection. Three other concentric AGWs in PMCs were 500–1000 km away from deep convection in the troposphere, while no convection was observed related to the wave on 29 July 2009. We perform a 2-D ray tracing study for the AGW event on 13 July 2007. The calculated propagation distance is much shorter than the distance between the AGWs in PMCs and the observed convection. The 2-D ray tracing study indicates that the AGWs in PMCs and in the stratosphere are probably excited by different tropospheric convective systems.

1. Introduction

Noctilucent clouds (NLCs, for ground-based observations) or polar mesospheric clouds (PMCs, for space observations) are tenuous ice clouds observed in the cold summer mesopause region at ~82–84 km, and form when the temperature drops below ~150 K. For over 100 years, NLCs have been sighted from the ground at latitudes of 50–65° during twilight hours when the solar depression angle ranges from ~6 to 15° [e.g., *Witt*, 1962; *Gadsden and Schröder*, 1989; *Thomas*, 1991]. NLCs display a variety of complex spatial structures, reflecting the broad spectrum of dynamics in the polar summer mesosphere. For example, bands, defined as long parallel streaks [*Haurwitz and Fogle*, 1969; *Gadsden and Parviainen*, 1995; *Taylor et al*., 2011], are similar to the bands commonly observed in the mesospheric airglow emissions [e.g., *Taylor*, 1986]. They are caused by upward propagating or ducted atmospheric gravity waves (AGWs) that modulate the PMCs or nightglow emissions [*Hines*, 1968]. Another commonly seen PMC feature, billows, defined as small-scale wave patterns with horizontal spacing of 3–10 km, are considered as dynamical or convective instabilities that are created by strong localized regions of wind shear or by breaking AGWs [*Fritts et al*., 1993].

From space, PMCs can be viewed at any local time with extensive spatial coverage. Since the launch of the NASA Aeronomy of Ice in the Mesosphere (AIM) satellite in April 2007 [*Russell et al*., 2009], ultraviolet (UV) images of PMCs with high spatial resolution have been taken by the Cloud Imaging and Particle Size (CIPS) instrument [*McClintock et al*., 2009] on board AIM. This has led to the discovery of previously unobserved PMC structures and allowed the study of PMC morphology in finer detail. Other than the known Type I, II, and IV types (i.e., Veils, Bands, and Whirls) of NLCs [*Gadsden and Parviainen*, 1995], structures such as "Voids," "Ice Rings," "Fronts," and "Vortex-like structures" have also been identified in these space-based images [*Rusch et al*.,

2009; *Thurairajah et al.*, 2012]. Fronts structures have also been observed in NLCs using ground-based images [*Dubietis et al.*, 2011; *Dalin et al.*, 2013].

This paper focuses on the study of one particular type of AGW, concentric AGWs, observed in PMCs by CIPS. Concentric AGWs have been observed in mesopause nightglow emissions from ground-based airglow imagers [e.g., *Taylor and Haphood*, 1988; *Sentman et al.*, 2003; *Suzuki et al.*, 2007; *Yue et al.*, 2009] and in the 4.3 and 15 μm CO_2 radiance images in the stratosphere from satellites [e.g., *Dewan et al.*, 1998; *Alexander and Teitelbaum*, 2007; *Eckerman et al.*, 2007; *Hoffmann and Alexander*, 2010; *Gong et al.*, 2012]. Because of their (partially) circular shapes, concentric AGWs are often associated with sources that exhibit approximate cylindrical symmetry, such as deep convection in the troposphere [e.g., *Taylor and Haphood*, 1988; *Dewan et al.*, 1998; *Yue et al.*, 2009; *Hoffmann and Alexander*, 2010] or earthquakes and tsunamis [*Tsugawa et al.*, 2011]. Recently, *Yue et al.* [2013] reported concurrent convective AGWs in the stratosphere and the mesopause region using joint observations by an airglow imager in Colorado and the Atmosphere Infrared Sounder (AIRS) on board the NASA Aqua satellite. Ground-based airglow imager observations in the mesosphere may be hindered by cloudy weather associated with the AGW-genesis deep convection, whereas AIRS favorably observes large-scale AGWs. CIPS provides PMC images with an unprecedented high spatial resolution (5 km) and allows the study of small-scale concentric AGW structures embedded in PMCs from space without the interference of bad weather.

In this paper, we report five concentric AGW events in PMCs observed by CIPS during the 2007 and 2009 Northern Hemisphere (NH) PMC seasons. Their possible convective sources are investigated using the AIRS and Infrared Atmospheric Sounding Interferometer (IASI) data. We present the first use of multisatellite data to study the coupling between the troposphere, stratosphere, and polar mesosphere via excitation and propagation of AGWs. The results from a 2-D ray tracing model are compared to the observations.

2. Instrumentation

2.1. CIPS

AIM is in a near-circular (~600 km altitude), 12:00 A.M./P.M. Sun-synchronous polar orbit [*Russell et al.*, 2009]. On board AIM, CIPS, a nadir-viewing panoramic imager, consists of an array of four charge-coupled device cameras each with detector filters centered at 265 nm with a 15 nm passband and having a 120° × 80° combined field of view. A detailed description of the CIPS instrument was given by *McClintock et al.* [2009]. CIPS images are ~1000 km across track by ~2000 km along track. Twenty-seven overlapping images are combined to yield orbit swaths that span ~9000 km in length. Approximately 15 PMC swaths are obtained each day, covering the polar cap between ~65° and 85° latitude. Because of the noon-midnight Sun-synchronous geometry of the AIM orbit, only two local solar times (LST)—around 22:00 LST and 14:00 LST—are sampled except for the highest latitudes where the satellite transitions between the ascending and descending nodes [*Lumpe et al.*, 2013].

PMC properties from the version 4.20, level 2 data (albedo, particle radius, and ice water content (IWC)) with 25 km^2 spatial resolution are used in this study. The Rayleigh scattered background is removed from the total radiance to retrieve the PMC scattered radiance [*Bailey et al.*, 2009; *Lumpe et al.*, 2013]. Detailed descriptions of the data products and retrieval and calibration algorithms can be found at the CIPS website: http://lasp.colorado.edu/aim/documentation.html. The CIPS albedo data analyzed here are defined as the ratio of the PMC scattered radiance to the incoming solar irradiance. The solar irradiance used in producing the CIPS database was calculated by integrating the Upper Atmosphere Research Satellite SoLar Stellar Irradiance Comparison Experiment spectrum (http://lasp.colorado.edu/lisird/uars/uars_ssi/index.html) [*Rottman and Woods*, 1994] over the CIPS bandpass. IWC is defined as the cloud ice mass per unit area of atmospheric air. Retrieved particle radius is defined as the mean radius for a Gaussian distribution of particles. An error analysis of CIPS measurements has been provided by *Lumpe et al.* [2013]. CIPS data evaluation is described by *Benze et al.* [2009, 2011]. Because of the finite thickness of the OH layer (8–9 km), airglow perturbations caused by short AGWs partially cancel out [*Swenson and Gardner*, 1998]. As the PMC layer is thinner (~5 km depth) [*Hervig and Gordley*, 2010], an advantage of the CIPS measurement over airglow imagers is that AGWs with shorter vertical wavelengths (<10 km) can be observed without cancelation between different wave phases at different heights.

2.2. AIRS and IASI

Like AIM, the Aqua satellite operates in a Sun-synchronous, near polar orbit at an altitude of 705 km. AIRS, a grating spectrometer, measures the thermal emission of atmospheric constituents in the nadir and sublimb

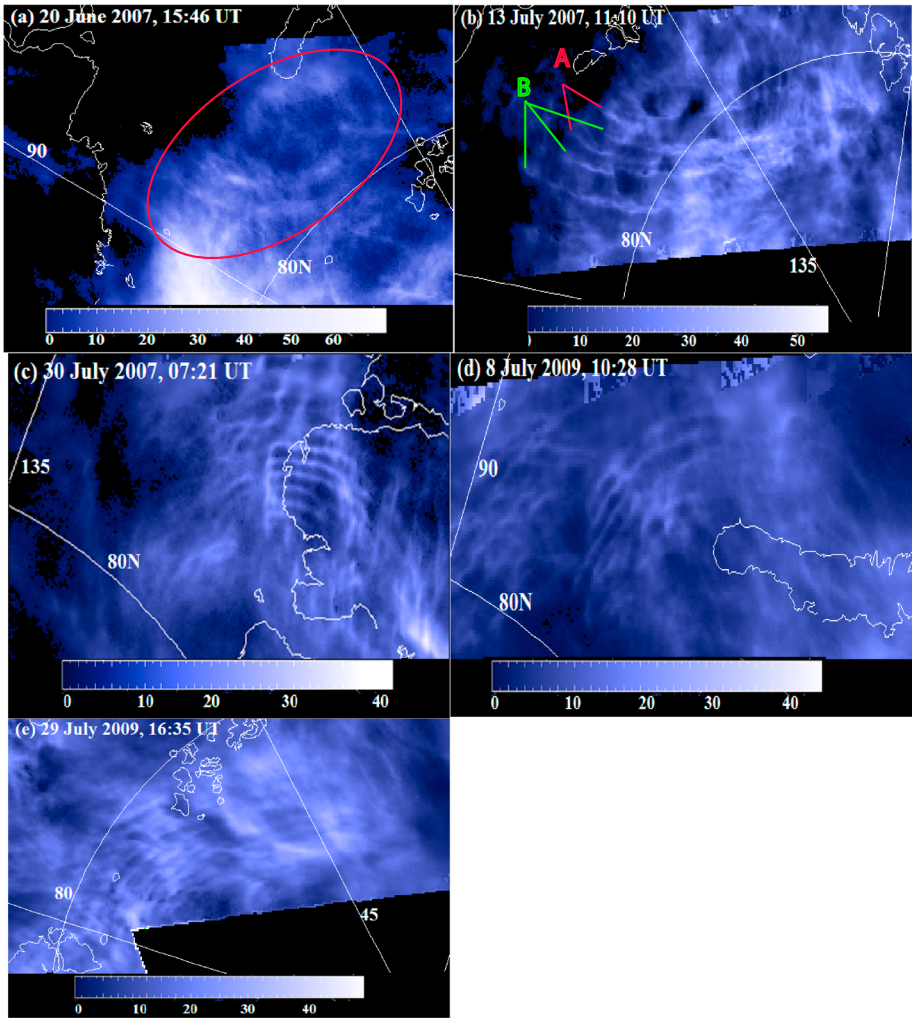

Figure 1. CIPS PMC albedo images (in units of 10^{-6} sr^{-1}) showing concentric AGWs in northern summers 2007 and 2009. The sizes of the images and the color scales have each been scaled differently to emphasize the concentric AGW structures. The characteristics of these AGWs are given in Table 1. (a–e) Wave events 1–5. In Figure 1b, there are two groups of AGWs overlaying on each other, denoted by A (red) and B (green).

viewing geometry [*Aumann et al.*, 2003]. In this current study, a subset of 42 AIRS channels covering the 4.3 μm CO_2 fundamental band is used to search for convective AGWs in the stratosphere near 30–40 km [*Hoffmann and Alexander*, 2010; *Hoffmann et al.*, 2013; *Yue et al.*, 2013]. The vertical weighting function for these channels has a full width half maximum of ~25 km. However, due to the low noise of the averaged 4.3 μm radiances, AGWs with vertical wavelengths as short as 10–15 km can be detected. Compared to CIPS, AIRS has a coarser spatial resolution and only AGWs with horizontal wavelengths longer than ~50 km can be seen. A detailed description of the AIRS measurements of stratospheric AGWs can be found in *Hoffmann and Alexander* [2010] and *Hoffmann et al.* [2013]. Furthermore, AIRS brightness temperature measurements at 8.1 μm (1231 cm^{-1}) can be compared to the tropopause temperature to identify deep convection [*Aumann et al.*, 2006; *Hoffmann and Alexander*, 2010; *Yue et al.*, 2013]. This is an efficient way to search for convective sources in remote regions or over the ocean where Doppler weather radar data are not available [*Yue et al.*, 2013]. For the AIRS nadir track, the equatorial crossing occurs at 13:30 LST (ascending orbit) and 01:30 LST (descending orbit).

To search for convective plumes at other local times, the 8.1 μm radiance measurements by IASI on the Meteorological Operation (MetOp)-A satellite [*Hilton et al.*, 2012] are analyzed in the same way as AIRS. As Aqua is in the afternoon orbit, MetOp provides coverage in the Sun-synchronous morning orbit.

Table 1. Observation Times and Locations of the Concentric AGW Events in CIPS in 2007 and 2009[a]

Orbit Number	Approximate Location	Approximate Time Near AGWs (UT)	Dominant Azimuth	λ_H (km)[b]	A_{ALB} ($\times 10^{-6}$ sr^{-1})[c]	A_{IWC} (g/km^2)[d]
(1) 832	79°N, 75°E	20 June (day 171) 2007 15:46	N-NE	70	5 (33%)	24 (29%)
(2) 1172[e]	80°N, 150°E	13 July (day 194) 2007 11:10	E	120–150	N/A	N/A
(3) 1423	76°N, 110°E	30 July (day 211) 2007 07:21	S-E	30	3 (20%)	19 (22%)
(4) 11996	77°N, 78°E	8 July (day 189) 2009 10:28	E	35	4 (31%)	29 (27%)
(5) 12313	81°N, 60°E	29 July (day 210) 2009 16:35	S	35	3 (12%)	33 (20%)

[a]Their estimated horizontal wavelengths and wave amplitudes are also tabulated. Values in the brackets are percentages relative to the mean albedo and IWC within the AGW fields.
[b]λ_H, Dominant horizontal wavelength (± 5 km).
[c]A_{ALB}, Wave amplitudes of AGWs in PMC albedo (1×10^{-6} sr^{-1}).
[d]A_{IWC}, Wave amplitudes of AGW in ice water content (g/km^2).
[e]More than one center determined as discussed in the text.

The equator crossing time for the descending node is 09:30 LST and 21:30 LST for the ascending node. Because the IASI 4.3 μm measurements are ~3 times noisier than AIRS, convective AGWs cannot be clearly detected by IASI.

3. Observations

In the CIPS images, concentric AGWs are identified as coherent rings or extended arcs with at least two visible wave crests (bright albedo structures) that show large angular curvatures (>30°). This differentiates

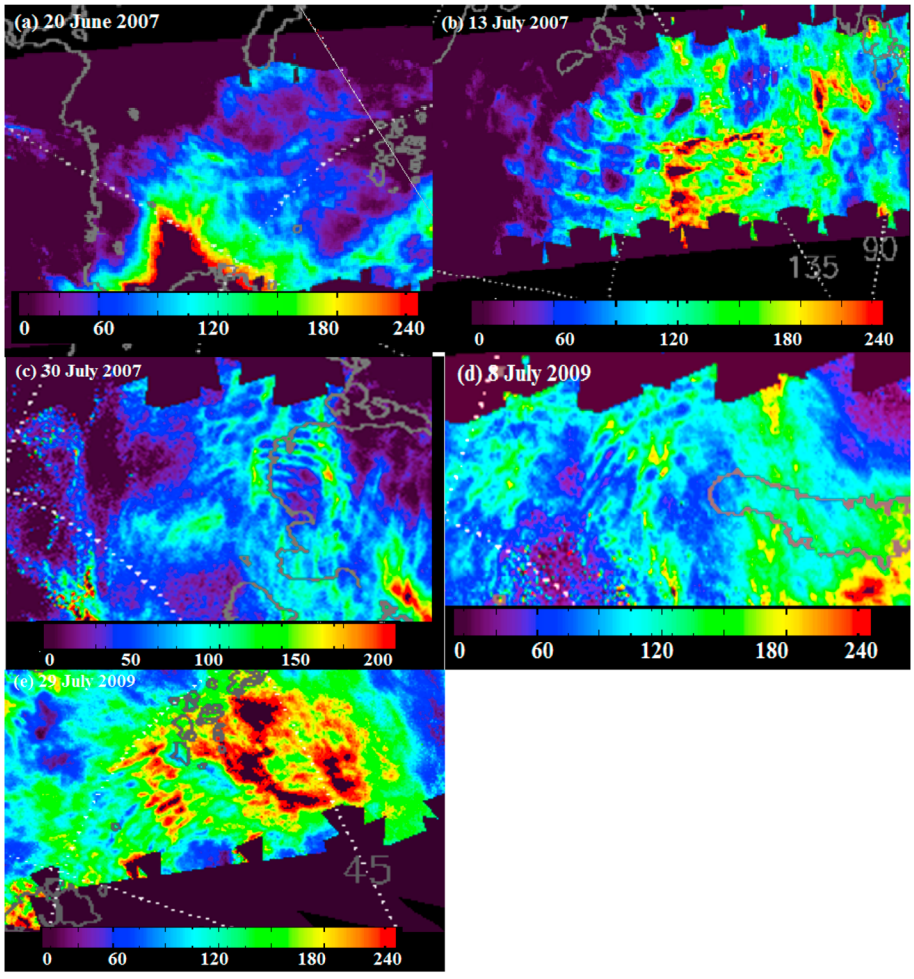

Figure 2. CIPS PMC ice water content images (g/km^2) showing concentric AGWs in northern summer 2007 and 2009 on the same maps as Figure 1. (a–e) Wave events 1–5.

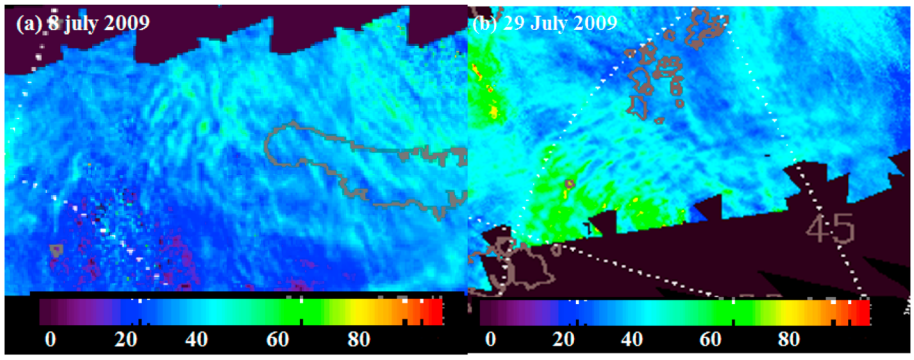

Figure 3. CIPS PMC particle radius (nm) showing concentric AGWs in northern summer 2009. (a) Wave event 4 and (b) wave event 5.

concentric AGWs from the recently discovered "ice rings" and "voids," which do not have coherent multiple concentric wave crests [*Rusch et al*., 2009; *Thurairajah et al*., 2012]. Based on a visual inspection of all the CIPS images between 2007 and 2012, five obvious concentric AGW events have been identified in 5 days in the 2007 and 2009 NH PMC seasons. (We have not yet found these concentric AGW events in the Southern Hemisphere (SH) or during the 2008 and 2010–2012 NH PMC seasons.) We note that none of the AGWs in Figure 1 are ideal circular structures or complete circles or ellipses. This indicates that both the wind filtering effect and source geometry effect might determine the final shape of the concentric AGWs in PMCs [e.g., *Alexander et al*., 1995; *Vadas et al*., 2009].

Table 1 lists their locations, estimated observational times, azimuths, and measured horizontal wavelengths. These events are identified by numbers 1–5 in the table. Figure 1 shows these five concentric wave patterns in the CIPS albedo images. Note that *Taylor et al*. [2011] first reported the AGWs in Figure 1b and suggested the possibility of determining their point sources. *Thurairajah et al*. [2012] also suggested that although the AGWs in Figure 1c look like billows, their horizontal wavelengths are much longer than the typical short wavelength of billows (i.e., $<$10 km), and thus identified them as small-scale waves. The observed concentric AGWs propagate either eastward or northward/southward. Since the background meridional wind is weak and the zonal wind is westward in northern summer [e.g., *Yue et al*., 2009], westward propagating AGWs would have been filtered by the mean wind.

AGWs in event #1 (Figure 1a) only have two visible wave crests (enclosed by the red oval). There are dim PMCs inside the concentric AGWs. The AGWs in event #2 (Figure 1b) are more complex and the outer arcs are not aligned with the inner arcs. Two groups of AGWs overlay each other, denoted by A and B in Figure 1b. Therefore, these AGWs have different apparent centers suggesting they were excited by different point sources. The horizontal wavelengths of AGWs A and B range from 120 to 150 km. In Figures 1c–1e (events #3, #4, and #5), the concentric AGWs exhibit very coherent patterns with multiple wave crests. Thus, their horizontal wavelengths, as short as 30 ± 5 km, can be measured with good accuracy (Table 1). Table 1 also lists

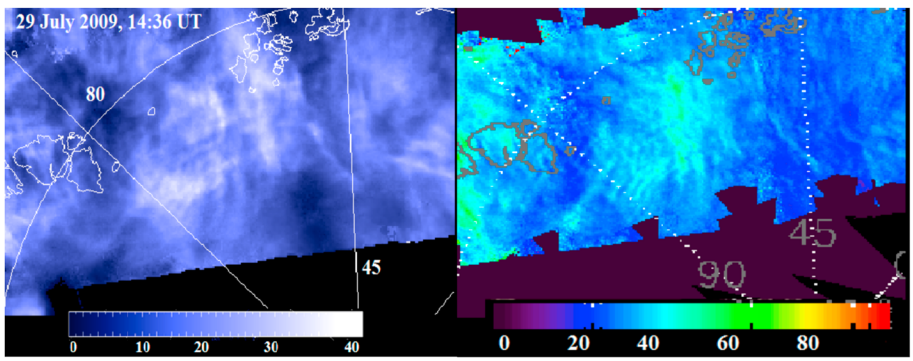

Figure 4. CIPS albedo and particle radius for orbit 12312 (wave event 5) at ~14:36 UT on 29 July 2009.

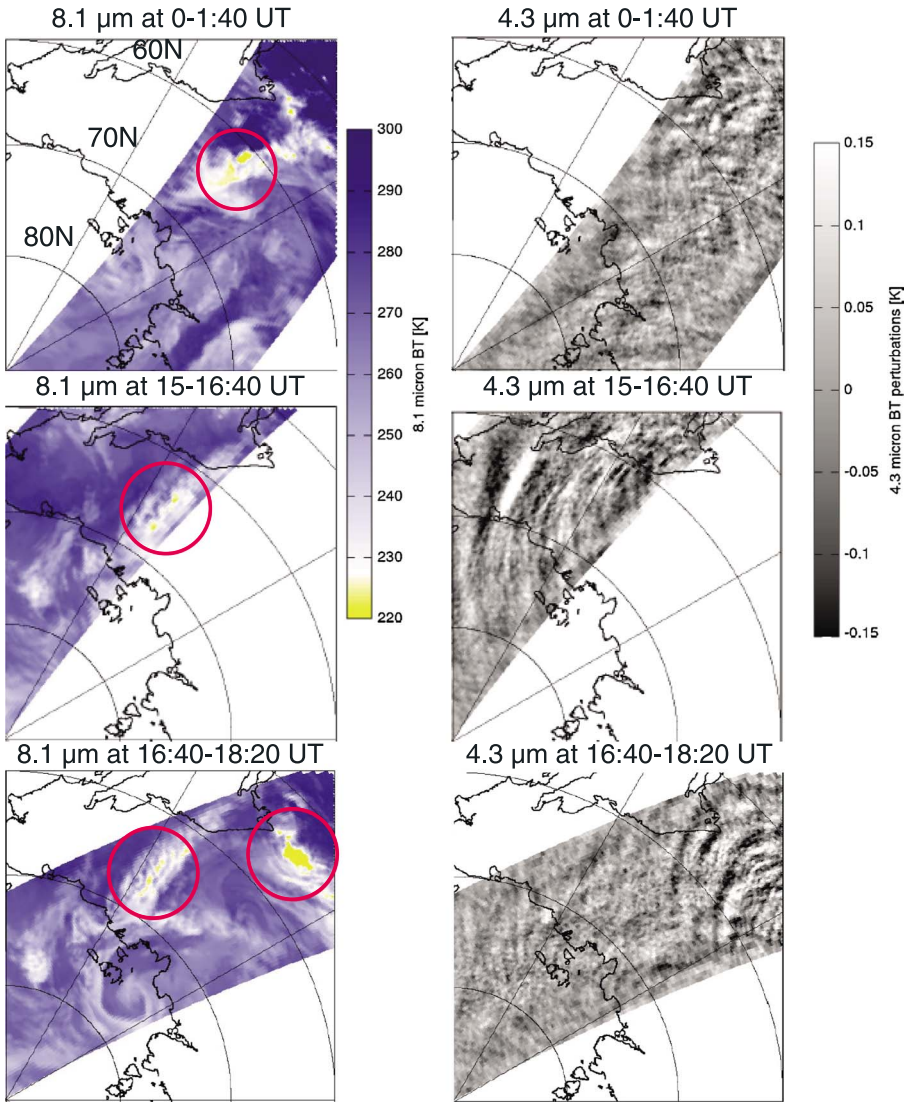

Figure 5. AIRS brightness temperature observations at (left column) 8.1 μm and (right column) 4.3 μm over Siberia (90°E–180°E, 50°N–90°N) on 13 July 2007. High clouds (yellow regions) are highlighted by red circles.

the individual absolute and relative wave amplitudes of the AGWs in the PMC Albedo and IWC. The average wave amplitudes of the PMC albedo images in Figures 1c–1e are approximately 3×10^{-6} sr^{-1} or ~ 20% of the mean albedo over the entire wave field. The "NA" for albedo and IWC measurements in Table 1 is due to overlapping rings; accurate characterization of these parameters is difficult.

Concentric AGWs in the PMC IWC are illustrated in Figure 2. By comparing to Figure 1, we can see that IWC is modulated by the AGWs with the same phase as the PMC albedo; i.e., the wave crests of the PMC albedo and IWC occur at the same locations. For AGW events #3, #4, and #5, the average amplitudes of AGWs in height integrated IWC are about 26 g/km^2 or 23% of the mean IWC. Figure 3 shows the PMC particle radius modulated by the AGW for events #4 and #5. The wave modulations in particle radius for the other three concentric AGWs events are not visually obvious. The average amplitude of particle radius modulation on 8 July 2009 and 29 July 2009 is 6 nm or 15%. Occasionally the same concentric AGWs can be seen in consecutive orbits, ~90 min apart. For example, Figure 4 shows CIPS orbit 12312 on 29 July 2009 around 14:30 UT. The concentric AGWs shown here at ~83°N and 60–90°E are the same as those for wave event #5 shown in Figures 1e and 3b for orbit 12313 at ~16:35 UT.

We have used the AIRS and IASI data to identify convective sources that possibly excited the concentric AGWs in PMCs. Figure 5 shows the AIRS brightness temperature at 4.3 μm and 8.1 μm on 13 July 2007 at three

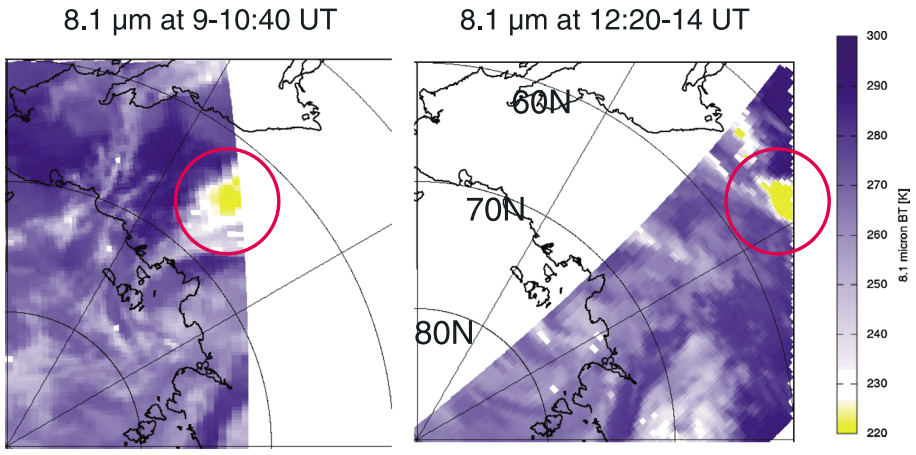

Figure 6. IASI observations of brightness temperature at 8.1 μm projected onto the same map as Figure 5 on 13 July 2007.

different times. The top left panel of the 8.1 μm brightness temperature illustrates the existence of cold (<225 K), high clouds (highlighted by the red circle) over central Siberia (~140°E, 70–75°N) at 00:00–01:40 UT. The climatological tropopause temperature is 225 K in the summer Arctic region [*Highwood et al.*, 2000]. Thus, clouds colder than 225 K (area in yellow color) likely penetrated the tropopause. The middle left panel shows that the convective system moved to the north and east ~15 h later. The middle right panel showing the 4.3 μm brightness temperature perturbation displays concentric AGWs emanating eastward (E) and northeastward (NE) at ~30–40 km altitude during 15:00–16:40 UT over eastern Siberia with estimated centers near the convective system. The horizontal wavelengths of the outermost AGWs are as large as ~200–400 km. The lower left panel not only shows the same cold clouds at 150°E but also another convective cell south of 60°N at 16:40–18:20 UT. Concentric AGWs are also seen over southern Siberia. Figure 5 demonstrates that the large convective system over Siberia lasted from 00:00 to 18:00 UT on 13 July 2007 and continuously excited concentric AGWs propagating into the stratosphere. We note here that although thunderstorms occur less frequently at high latitudes as compared to the tropics and midlatitudes, there are still plenty of convective events happening in the Siberia summer, especially in July [*Mullayarov et al.*, 2009, 2010]. Figure 1b shows similar concentric AGWs in PMCs at 11:10 UT on the same day that were aligned with the

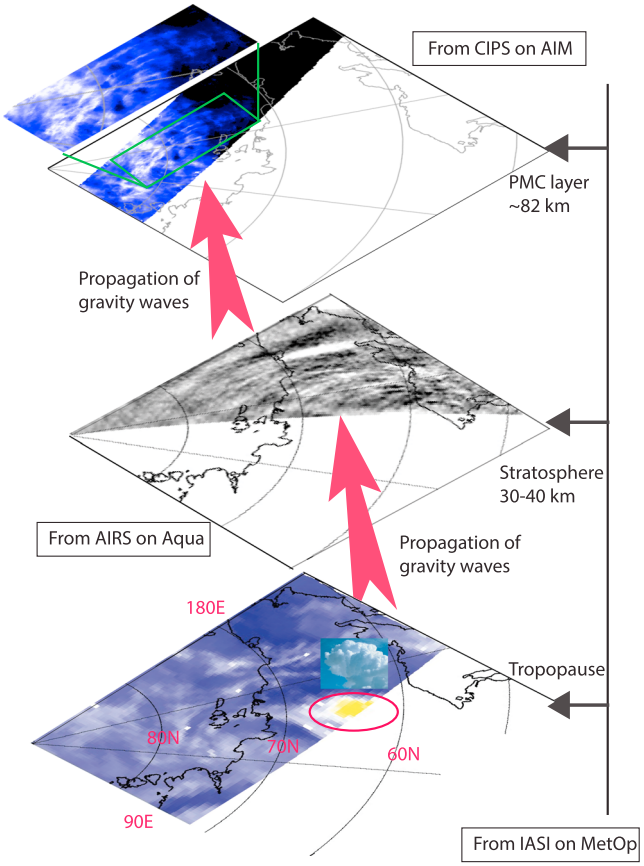

Figure 7. Three panels showing the coupling of the troposphere and polar mesopause via the excitation and propagation of AGWs on 13 July 2007. (top) IASI brightness temperature at 8.1 μm at 09:00–10:40 UT, (middle) AIRS brightness temperature at 4.3 μm at 15:00–16:40 UT, (bottom) CIPS albedo image for event 2 on orbit 1172 (the same orbit as Figure 1b) around 11:10 UT in the northern polar region.

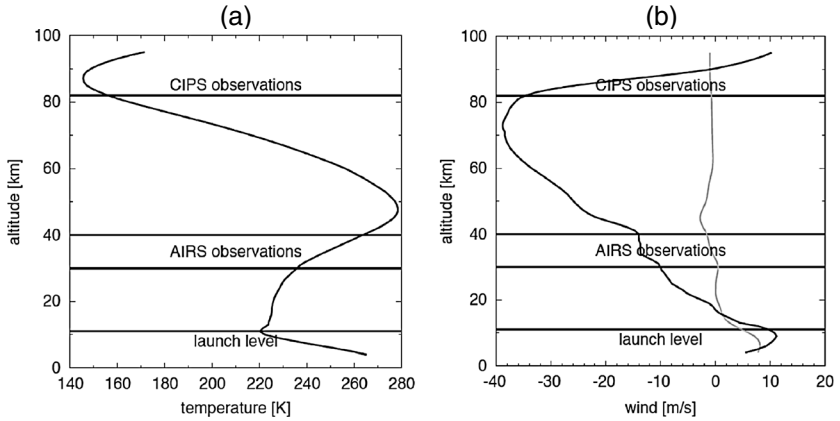

Figure 8. Profiles of (a) temperature and (b) zonal (black) and meridional (grey) winds on 13 July 2007. The temperature profile is composed of the CIRA-86 profile above 50 km and the average of ERA-Interim data at 135–180°E and 60–70°N at 12 h below 50 km. The wind profiles are resembled by ERA-Interim below 50 km and TIME-GCM July climatology wind above 50 km. The black line at 11 km denotes the AGW launch level. The two black lines at 30 and 40 km indicate a layer where the 4.3 μm CO_2 band becomes optically thick and the AIRS brightness temperatures are measured. The black line at 82 km denotes the height of the PMC layer.

stratospheric AGWs in Figure 5, but with different apparent centers. To search for coincident high convective clouds responsible for these AGWs in PMCs, Figure 6 shows the IASI observations of brightness temperature at 8.1 μm on 13 July 2007. Another deep convection system south of 60°N is also clearly shown in the IASI image at 12:20–14:00 UT.

We overlay the plots from Figures 1, 5, and 6 for wave event #2 at different layers in Figure 7 to illustrate the troposphere-stratosphere-mesosphere coupling via the excitation and propagation of convective AGWs. The top panel of Figure 7 shows the CIPS albedo around 11:00 UT. The middle panel indicates AGW activity in the stratosphere at 15:00–16:40 UT, and the bottom panel suggests high clouds in the troposphere at 09:00–10:40 UT. Most likely, had AIRS observed this region earlier (i.e., around 11 UT), it would still have seen the stratospheric AGWs. Figure 7 illustrates that the concentric AGWs in CIPS align well with the stratospheric AGWs in AIRS. Both wavefronts were emanating eastward and northeastward. However, the estimated center for the waves in PMCs (70°–80°) is further north of the center for the stratospheric waves (~65°). And the AGWs in the mesosphere were observed 4–5 h earlier by CIPS than those in the stratosphere by AIRS. This indicates that both AGWs are likely propagating upward from convective sources, but they were not excited by the same convective system. The propagation of AGWs through different layers was also investigated numerically using a ray tracing model (see section 4).

The IASI 8.1 μm measurements were also used to search for deep convection related to the concentric AGWs seen in CIPS with better temporal coincidence. Except for AGW event #5 on 29 July 2009, simultaneous deep convective clouds that are colder than 225 K are found 500–1000 km away from the estimated AGW centers (not shown). Neither AIRS nor IASI observations show evidence for convection anywhere in the northern polar region during the AGW #5 event on 29 July 2009.

4. Linear 2-D Ray Tracing of AGWs

To further understand the AGW propagation from the tropopause into the upper mesosphere, we apply a linear ray trace 2-D model to wave event #2 that occurred on 13 July 2007. *Yue et al.* [2013] used the same model to study the propagation of concentric AGWs seen by an airglow imager and AIRS. The model was first described in *Alexander* [1996, 1998]. The model includes the dispersion relation with the effects of rotation at low frequencies and nonhydrostatic effects at higher frequencies. The background atmosphere is composed of reanalysis and model data. Figure 8a shows temperature profiles assembled from CIRA-86 (The Committee on Space Research International Reference Atmosphere) above 50 km and ERA-Interim for 13 July 2007 below 50 km. Figure 8b shows the zonal and meridional winds, composed of ERA-Interim below 50 km and National Center for Atmospheric Research Thermosphere-Ionosphere-Mesosphere-Electrodynamics General Circulation Model (TIME-GCM) July climatology for wind above 50 km [*Roble*, 1995].

Table 2. Ground-Based Phase Speeds c_0, Ground-Based Periods $2\pi/\omega_0$, Vertical Wavelengths $2\pi/m_L$, and Horizontal Wavelengths $2\pi/k$ Used for Six AGWs Launched at the Tropopause in the Ray Tracing Simulation

	Vertical Wavelengths $2\pi/m_L$	
Horizontal Wavelengths $2\pi/k$	11 km	22 km
120 km	$c_0 = 45$ m/s, $2\pi/\omega_0 = 44$ min	$c_0 = 77$ m/s, $2\pi/\omega_0 = 26$ min
200 km	$c_0 = 45$ m/s, $2\pi/\omega_0 = 74$ min	$c_0 = 78$ m/s, $2\pi/\omega_0 = 43$ min
400 km	$c_0 = 46$ m/s, $2\pi/\omega_0 = 146$ min	$c_0 = 78$ m/s, $2\pi/\omega_0 = 85$ min

Six monochromatic eastward propagating AGWs are launched above the tropopause at 11 km in the model. Theoretical considerations and calculations are designed to constrain the ray tracing parameters. Due to the strong westward wind in Figure 8, only eastward propagating waves with fairly high phase speeds and long enough vertical wavelengths are visible in the AIRS data in the stratosphere [*Hoffmann and Alexander*, 2010]. The horizontal wavelengths are selected as 120 km (CIPS observed AGWs), and 200 km and 400 km (AIRS AGWs). To estimate the vertical wavelength, we assume the convective source extends over approximately the full depth of the troposphere or ~11 km. Thus, the deepest tropospheric vertical wavelengths λ_z emanating from the convective source are estimated to be 22 km (2 × 11 km) to 44 km (4 × 11 km) [*Holton et al.*, 2002]. When these waves cross the tropopause, their vertical wavelengths decrease by a factor of $2 = N_s/N_t$, where $N_s = 0.02\ s^{-1}$ (stratospheric buoyancy frequency) and $N_t = 0.01\ s^{-1}$ (tropospheric buoyancy frequency). This follows from the simplified dispersion relation for medium frequency AGWs [*Fritts and Alexander*, 2003],

$$|m| = \frac{N}{|\hat{c}_h|} \tag{1}$$

where $m = 2\pi/\lambda_z$ is the vertical wave number, and $\hat{c}_h$ is the intrinsic phase speed. At the launch level above the tropopause, we assume vertical wavelengths ranging from 11 to 22 km for some of the fastest waves. We choose two vertical wavelengths, 11 km and 22 km for the calculations and used the medium frequency AGW dispersion relationship,

$$\omega^2 = \frac{N^2k^2 + f^2(m^2 + \alpha^2)}{m^2 + k^2 + \alpha^2} \tag{2}$$

where $\alpha = 1/2H$, $H = 7$ km (scale height), $f = 2\Omega\sin(65°)$ (Coriolis parameter $= 1.322 \times 10^{-4}\ s^{-1}$), k is horizontal wave number ($2\pi/120$ km, $2\pi/200$ km, and $2\pi/400$ km), and ω is intrinsic frequency. Taking the background

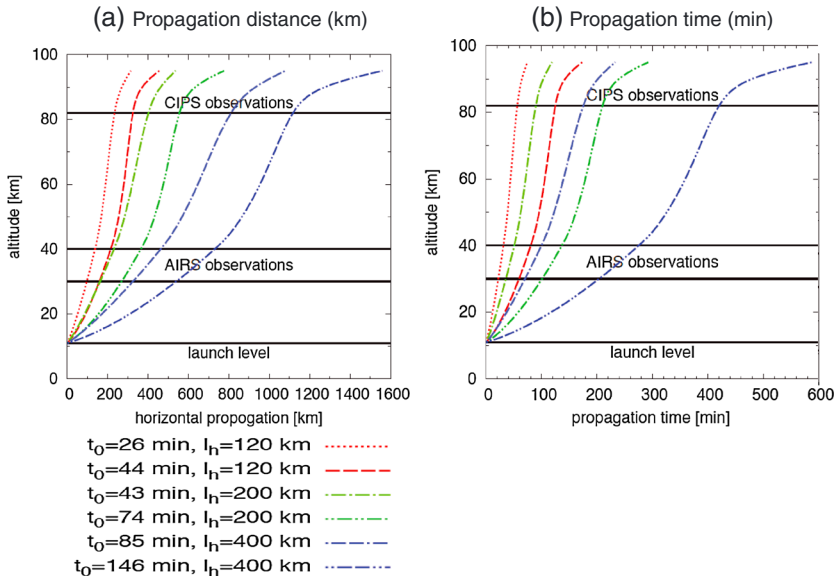

Figure 9. (a) Horizontal propagation distance and (b) propagation time from the launch level to the upper mesosphere for six AGWs. The parameters for these AGWs are displayed below. AGWs with the same horizontal wavelength but different vertical wavelengths (11 km and 22 km) have the same color.

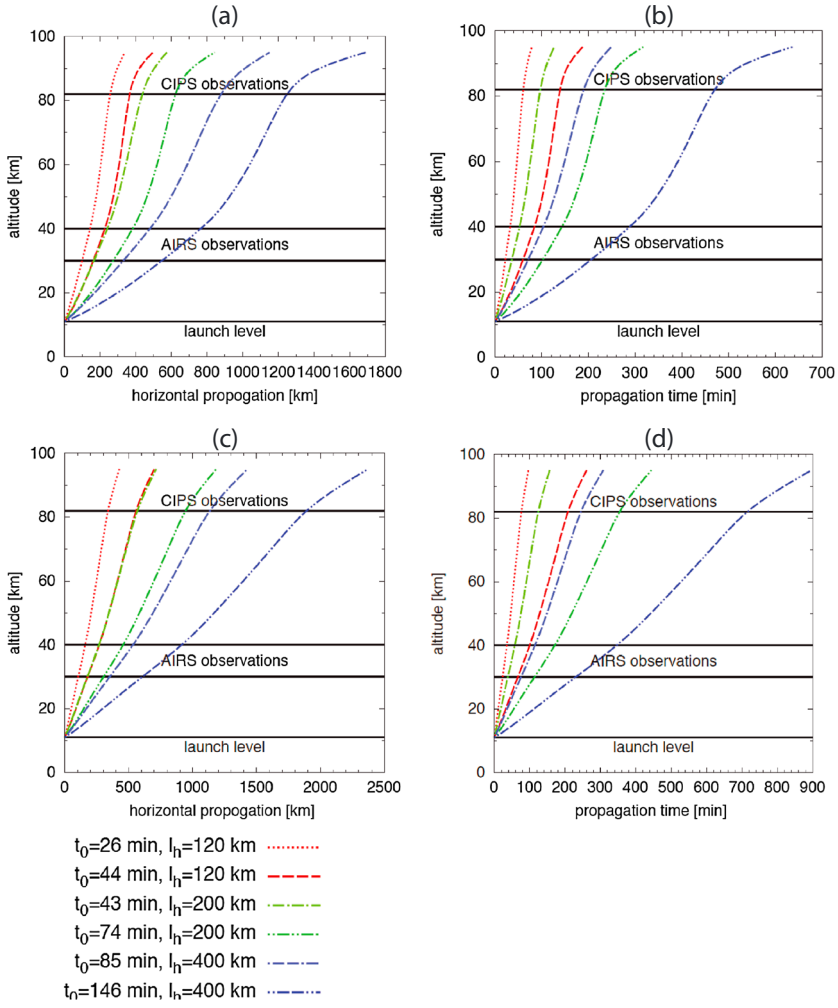

Figure 10. (a and c) Horizontal propagation distance and (b and d) propagation time from the launch level to the upper mesosphere for the same six AGWs in Figure 9. Figures 10a and 10b for northeastward propagating waves, Figures 10c and 10d for northward propagating waves. AGWs with the same horizontal wavelength but different vertical wavelengths (11 km and 22 km) have the same color.

zonal wind at launch level as $U_L = 10$ m/s, the ground-based phase speeds and ground-based periods can be calculated as indicated in Table 2. A reasonable range of ground-based phase speed is 45–78 m/s, which enables the detection of AGWs by AIRS.

Figure 9 exhibits the horizontal propagation distances and propagation times to shed some light on the spatial and temporal relationships between the AIRS and CIPS observed AGWs and high clouds. For the run with 44 min period and horizontal wavelength of 120 km, the AGW travels horizontally about 300 km from the source to the PMC layer in about 120 min, as shown in Figure 9a. Thus, the AGWs observed by CIPS at ~11 UT were likely excited around 9 UT. On the other hand, the travel distance is too short compared to the actual distance of ~1000 km between the AGWs in CIPS and the convective source. This discrepancy will be discussed in the next section. Moreover, it takes as long as ~600–800 km and 220–280 min (or about 4 h) for the 400 km and 146 min AGWs (the outermost waves in the middle panel of Figure 7) traveling from the tropopause to the CO_2 layer. The AGWs observed by AIRS at 15:00–16:40 UT were likely excited at ~11:00–12:40 UT.

As for circular waves, the wind relative to the wave propagating azimuth (listed in Table 1) could be important. We performed further sensitivity studies to examine the observed wave propagation deviating from the eastward direction. Figure 10 shows the propagation time and distance for the northeastward and

northward propagating AGWs but with the same wave parameters. The propagation time and distance for the northeastward waves are slightly greater than those going eastward. On the other hand, the northward waves travel ~50% longer distance and time compared to the eastward waves. Nevertheless, various propagation distances associated with different propagation directions cannot account for the discrepancies between the location of the convective sources and the concentric AGW event #2 in PMCs.

5. Discussion

Ever since, it was recognized that the association of concentric AGWs in the stratospheric CO_2 radiance [*Dewan et al*., 1998] and airglow emissions in the mesosphere and lower thermosphere (MLT) [*Taylor and Haphood*, 1988] is associated with strong isolated thunderstorm activity, subsequent concentric wave studies have always shown strong correlation, both spatially and temporally, with underlying deep convection [e.g., *Dewan et al*., 1998; *Sentman et al*., 2003; *Suzuki et al*., 2007; *Hoffmann and Alexander*, 2010; *Grimsdell et al*., 2010; *Yue et al*., 2009, 2013; *Vadas et al*., 2012]. This correlation has also been demonstrated using numerical models [e.g., *Grimsdell et al*., 2010; *Yue et al*., 2013; *Vadas et al*., 2012]. However, in this paper, we have discovered a few mesospheric concentric AGWs (e.g., wave event 5) in the Arctic far away from tropospheric convection even though we have used two satellite data sets with broader local time coverage (AIRS and IASI). On the other hand, the temporal and spatial correlation between the stratospheric AGWs in AIRS measurements and deep convection in AIRS and IASI is evident. Given a low time and spatial resolution of the AIRS and IASI images (several hours apart), it is possible that there was a small convective event near 75°N, 130°E at 09:00 UT, which was missed by AIRS and IASI. In this case, the horizontal travel distance to the mesopause would be about 300 km, with a propagation time of 120 min that agrees very well with the blue model curve (44 min, 120 km) in Figure 9. Thus, one can see that there are large uncertainties in determining the position and time of the convective source due to low time resolution of the AIRS and IASI data.

Another possible reason for the absence of convective sources near concentric AGWs is simply that there might exist other unknown concentric AGW sources in the polar region. One candidate is large earthquakes/tsunamis [*Tsugawa et al*., 2011]. However, there were no major earthquakes in the Arctic during these 6 days shown in the U. S. Geological Survey database (http://earthquake.usgs.gov). Another possible source is secondary AGWs from the breaking of primary AGWs [*Zhou* et al., 2002]. But the breaking of primary AGWs may not necessarily form a point source. More substantial observational work is necessary to reveal if there are any unidentified AGW sources in the polar regions.

6. Conclusions

In this paper, we present new observations of concentric AGWs in simultaneous CIPS images of PMC albedo, IWC, and particle radius. Altogether there were five obvious concentric ring events detected in the 2007 and 2009 NH PMC seasons. No similar events were found in the SH or during other years. It is possible that there are other concentric AGWs in CIPS albedo images that are too dim to be easily identified by visual inspection of the images. The five AGWs exhibited horizontal wavelengths varying from 30 to 120 km, which are typical of short and medium period AGW observed in the MLT nocturnal airglow emissions [e.g., *Ejiri et al*., 2003]. The AGW events #3, #4, and #5 on 30 July 2007, 8 July 2009, and 29 July 2009 are more coherent. They have average amplitudes of $3 \times 10^{-6}\,\mathrm{sr}^{-1}$, 26 g/km^2, and 6 nm in albedo, IWC, and particle radius, respectively. AGWs (event #2) on 13 July 2007 have two apparent centers.

We have investigated the possible upper troposphere convective origin of the concentric AGW event #2 on 13 July 2007 by inspecting concurrent AIRS and IASI images. Aligned circular wave patterns in both the AIRS 4.3 μm band at ~30–40 km and CIPS PMC images at ~82 km suggest the upward propagation of AGWs from deep convection occurring in the troposphere over Siberia through the stratosphere into the mesopause region. Linear ray tracing simulations were performed to show that stratospheric AGWs in AIRS are highly correlated with the tropospheric convection. However, the AGWs in PMCs are too far away from the source region to see a similar correlation. The absence of convective sources adjacent to other concentric AGW events may have been due to another unidentified AGW source in the polar regions or simply incorrect assumptions about the sources or propagation conditions.

Acknowledgments

The NASA AIM mission is under contract NAS5-03132. AIM was developed as part of the NASA Small Explorer Project. The authors acknowledge the efforts of the AIM CIPS data processing and science teams. AIRS data are distributed by the NASA Goddard Earth Sciences Data Information and Services Center. IASI data were obtained from the British Atmospheric Data Center. J.Y. is grateful for the discussions with John McNabb, Jerry Lumpe, and Kris Bedka on an early version of the draft. We are grateful to three reviewers and David Rusch for helpful comments.

References

Alexander, M. J. (1996), A simulated spectrum of convectively generated gravity waves: Propagation from the tropopause to the mesopause and effects on the middle atmosphere, *J. Geophys. Res.*, *101*(D1), 1571–1588, doi:10.1029/95JD02046.

Alexander, M. J. (1998), Interpretations of observed climatological patterns in stratospheric gravity wave variance, *J. Geophys. Res.*, *103*(D8), 8627–8640, doi:10.1029/97JD03325.

Alexander, M. J., and H. Teitelbaum (2007), Observation and analysis of a large amplitude mountain wave event over the Antarctic Peninsula, *J. Geophys. Res.*, *112*, D21103, doi:10.1029/2006JD008368.

Alexander, M. J., J. R. Holton, and D. R. Durran (1995), The gravity wave response above deep convection in a squall line simulation, *J. Atmos. Sci.*, *52*, 2212–2226.

Aumann, H. H., et al. (2003), AIRS/AMSU/HSB on the Aqua mission: Design, science objective, data products, and processing systems, *IEEE Trans. Geosci. Remote Sens.*, *41*, 253–264.

Aumann, H. H., D. Gregorich, and S. M. DeSouza-Machado (2006), AIRS observations of deep convective clouds, *Proc. SPIE*, *6301*, 63010J, doi:10.1117/12.681201.

Bailey, S. M., et al. (2009), Phase functions of polar mesospheric cloud ice as observed by the CIPS instrument on the AIM satellite, *J. Atmos. Sol. Terr. Phys.*, *71*, 373–380.

Benze, S., et al. (2009), Comparison of polar mesospheric clouds measurements from the Cloud Imaging and Particle Size experiment and the solar backscatter ultraviolet instrument in 2007, *J. Atmos. Sol. Terr. Phys.*, *71*, 365–372.

Benze, S., C. E. Randall, M. T. DeLand, G. E. Thomas, S. M. Bailey, J. M. Russell III, and A. W. Merkel (2011), Evaluation of AIM CIPS measurements of polar mesospheric clouds by comparison with SBUV data, *J. Atmos. Sol. Terr. Phys.*, *73*, 2065–2072.

Dalin, P., et al. (2013), First common volume ground-based and space measurements of the mesospheric front in noctilucent clouds, *Geophys. Res. Lett.*, *40*, 6399–6404, doi:10.1002/2013GL058553.

Dewan, E. M., et al. (1998), MSX satellite observations of thunderstorm-generated gravity waves in mid-wave infrared images of the upper stratosphere, *Geophys. Res. Lett.*, *25*(7), 939–942, doi:10.1029/98GL00640.

Dubietis, A., et al. (2011), Noctilucent clouds: Modern ground-based photographic observations by a digital camera network, *Appl. Opt.*, *50*(28), F72–F79, doi:10.1364/AO.50.000F72.

Ejiri, M. K., K. Shiokawa, T. Ogawa, K. Igarashi, T. Nakamura, and T. Tsuda (2003), Statistical study of short-period gravity waves in OH and OI nightglow images at two separated sites, *J. Geophys. Res.*, *108*(D21), 4679, doi:10.1029/2002JD002795.

Eckerman, S. D., J. Ma, D. L. Wu, and D. Broutman (2007), A three dimensional mountain wave imaged in satellite radiance throughout the stratosphere: Evidence of the effects of directional wind shear, *Q. J. R. Meteorol. Soc.*, *133*(629), 1959–1975.

Fritts, D. C., and M. J. Alexander (2003), Gravity wave dynamics and effects in the middle atmosphere, *Rev. Geophys.*, *41*(1), 1003, doi:10.1029/2001RG000106.

Fritts, D. C., J. R. Isler, G. E. Thomas, and Ø. Andreassen (1993), Wave breaking signatures in noctilucent clouds, *Geophys. Res. Lett.*, *20*(19), 2039–2042, doi:10.1029/93GL01982.

Gadsden, M., and P. Parviainen (1995), Observing noctilucent clouds, International Association of Geomagnetism and Aeronomy. [Available at www.iugg.org/IAGA/iaga_pages/pdf/ONC_Sep06.pdf.]

Gadsden, M., and W. Schröder (1989), *Noctilucent Clouds*, Springer, Berlin.

Gong, J., D. L. Wu, and S. D. Eckermann (2012), Gravity wave variances and propagation derived from AIRS radiances, *Atmos. Chem. Phys.*, *12*(4), 1701–1720.

Grimsdell, A. W., M. J. Alexander, P. T. May, and L. Hoffmann (2010), Model study of waves generated by convection with direct validation via satellite, *J. Atmos. Sci.*, *5*, 1617–1631.

Haurwitz, B., and B. Fogle (1969), Wave forms in noctilucent clouds, *Deep Sea Res.*, *16*, 85–95.

Hervig, M. E., and L. L. Gordley (2010), Temperature, shape, and phase of mesospheric ice from Solar Occultation for Ice Experiment observations, *J. Geophys. Res.*, *115*, D15208, doi:10.1029/2010JD013918.

Highwood, E. J., B. J. Hoskins, and P. Berrisford (2000), Properties of the Arctic tropopause, *Q. J. R. Meteorol. Soc.*, *126*, 1515–1532.

Hilton, F., et al. (2012), Hyperspectral Earth observation from IASI: Five years of accomplishments, *Bull. Am. Meteorol. Soc.*, *93*, 347–370.

Hines, C. O. (1968), A possible source of waves in noctilucent clouds, *J. Atmos. Sci.*, *25*, 937–942.

Hoffmann, L., and M. J. Alexander (2010), Occurrence frequency of convective gravity waves during the North American thunderstorm season, *J. Geophys. Res.*, *115*, D20111, doi:10.1029/2010JD014401.

Hoffmann, L., X. Xue, and M. J. Alexander (2013), A global view of stratospheric gravity wave hotspots located with Atmospheric Infrared Sounder Observations, *J. Geophys. Res. Atmos.*, *118*, 416–434, doi:10.1029/2012JD018658.

Holton, J. R., J. H. Beres, and X. Zhou (2002), On the vertical scale of gravity waves excited by localized thermal forcing, *J. Atmos. Sci.*, *59*, 2019–2023.

Lumpe, J., et al. (2013), Retrieval of polar mesospheric cloud properties from CIPS: Algorithm description, error analysis and cloud detection sensitivity, *J. Atmos. Sol. Terr. Phys.*, *104*, 167–196, doi:10.1016/j.jastp.2013.06.007.

McClintock, W., et al. (2009), The cloud imaging and particle size experiment on the Aeronomy of Ice in the Mesosphere mission: Instrument concept, design, calibration, and on-orbit performance, *J. Atmos. Sol. Terr. Phys.*, doi:10.1016/j.jastp.2008.10.011.

Mullayarov, V. A., A. A. Toropov, V. I. Kozlov, and R. R. Karimov (2009), Patterns of spatial distribution of positive thunderstorm discharges in Eastern Siberia, *Russ. Meteorol. Hydrol.*, *34*(6), 364–370.

Mullayarov, V. A., V. I. Kozlov, A. A. Toropov, and R. R. Karimov (2010), Some results of observations of positive lightning discharges and relative phenomena in the east of Siberia, *J. Atmos. Sol. Terr. Phys.*, *72*(5-6), 409–418.

Roble, R. G. (1995), Energetics of the mesosphere and thermosphere, in *the Upper Mesosphere and Lower Thermosphere: A Review of Experiment and Theory*, *Geophys. Monogr. Ser.*, vol. 87, edited by R. M. Johnson and T. L. Killeen, pp. 1–20, AGU, Washington, D. C.

Rottman, G. J., and T. N. Woods (1994), Upper Atmosphere Research Satellite (UARS) Solar Stellar Irradiance Comparison Experiment (SOLSTICE), *Proc. SPIE*, *2266*, 317, doi:10.1117/12.187569.

Russell, J. M., III, et al. (2009), Aeronomy of Ice in the Mesosphere (AIM): Overview and early science results, *J. Atmos. Sol. Terr. Phys.*, doi:10.1016/j.jastp.2008.08.011.

Rusch, D. W., et al. (2009), The cloud imaging and particle size experiment on the Aeronomy of Ice in the Mesosphere mission: Cloud morphology for the northern 2007 season, *J. Atmos. Sol. Terr. Phys.*, doi:10.1016/j.jastp.2008.11.005.

Sentman, D. D., et al. (2003), Simultaneous observations of mesospheric gravity waves and sprites generated by a midwestern thunderstorm, *J. Atmos. Sol. Terr. Phys.*, *65*, 537–550, doi:10.1016/S1364-6826(02)00328-0.

Suzuki, S., K. Shiokawa, Y. Otsuka, T. Ogawa, K. Nakamura, and T. Nakamura (2007), A concentric gravity wave structure in the mesospheric airglow images, *J. Geophys. Res.*, *112*, D02102, doi:10.1029/2005JD006558.

Swenson, G. R., and C. S. Gardner (1998), Analytical models for the responses of the mesospheric OH* and Na layers to atmospheric gravity waves, *J. Geophys. Res.*, *103*, 6271–6294.

Taylor, M. J. (1986), TV observations of mesospheric wave structures, Collection of Works of the International Workshop of Noctilucent Clouds, Tallinn, Estonian SSR, USSR, August 1984, International Commission of Cloud Physics International Association of Meteorology and Atmospheric Physics, pub. in *Tallinn #Valgus*", pp. 153–172.

Taylor, M. J., and M. A. Haphood (1988), Identification of a thunderstorm as a source of short period gravity waves in the upper atmospheric nightglow emissions, *Planet Space Sci.*, *36*(4), 975–985.

Taylor, M. J., et al. (2011), High-latitude gravity wave measurements in noctilucent clouds and polar mesospheric clouds, in *Aeronomy of the Earth's Atmosphere and Ionosphere*, IAGA Special Sopron Book Series, vol. 2(1), pp. 93–105, Springer, Netherlands.

Thomas, G. E. (1991), Mesospheric clouds and the physics of the mesopause region, *Rev. Geophys.*, *29*(4), 553–575, doi:10.1029/91RG01604.

Thurairajah, B., et al. (2012), Morphology of polar mesospheric clouds as seen from space, *J. Atmos. Sol. Terr. Phys.*, doi:10.1016/j.jastp.2012.09.009.

Tsugawa, T., A. Saito, Y. Otsuka, M. Nishioka, T. Maruyama, H. Kato, T. Nagatsuma, and K. T. Murata (2011), Ionospheric disturbances detected by GPS total electron content observation after the 2011 off the Pacific coast of Tohoku Earthquake, *Earth Planets Space*, *63*, 875–879.

Vadas, S., J. Yue, C.-Y. She, P. Stamus, and A. Z. Liu (2009), A model study of the effects of winds on concentric rings of gravity waves from a convective plume near Fort Collins on 11 May 2004, *J. Geophys. Res.*, *114*, D06103, doi:10.1029/2008JD010753.

Vadas, S., J. Yue, and T. Nakamura (2012), Mesospheric concentric gravity waves generated by multiple convective storms over the North American Great Plain, *J. Geophys. Res.*, *117*, D07113, doi:10.1029/2011JD017025.

Witt, G. (1962), Height, structure, and displacements of noctilucent clouds, *Tellus*, *14*, 1–8.

Yue, J., et al. (2009), Concentric gravity waves in the mesosphere generated by deep convective plumes in the lower atmosphere near Fort Collins, Colorado, *J. Geophys. Res.*, *114*, D06104, doi:10.1029/2008JD011244.

Yue, J., L. Hoffmann, and M. J. Alexander (2013), Simultaneous observations of convective gravity waves from a ground-based airglow imager and the AIRS satellite experiment, *J. Geophys. Res. Atmos.*, *118*, 3178–3191, doi:10.1002/jgrd.50341.

Zhou, X.-L., J. R. Holton, and G. L. Mullendore (2002), Forcing of secondary waves by breaking of gravity waves in the mesosphere, *J. Geophys. Res.*, *107*(D7), doi:10.1029/2001JD001204.